

Two-dimensional nanoscale correlations in the strong negative thermal expansion material ScF_3 Sahan U. Handunkanda,^{1,2} Connor A. Occhialini,¹ Ayman H. Said,³ and Jason N. Hancock^{1,2,*}¹*Department of Physics, University of Connecticut, Storrs, Connecticut 06269, USA*²*Institute for Materials Science, University of Connecticut, Storrs, Connecticut 06269, USA*³*Advanced Photon Source, Argonne National Laboratory, 9700 S. Cass Ave., Argonne, Illinois 60439, USA*

(Received 13 June 2016; revised manuscript received 30 October 2016; published 7 December 2016)

We present diffuse x-ray scattering data on the strong negative thermal expansion (NTE) material ScF_3 and find that two-dimensional nanoscale correlations exist at momentum-space regions associated with possibly rigid rotations of the perovskite octahedra. We address the extent to which rigid octahedral motion describes the dynamical fluctuations behind NTE by generalizing a simple model supporting a single floppy mode that is often used to heuristically describe instances of NTE. We find this model has tendencies toward dynamic inhomogeneities and its application to recent and existing experimental data suggest an intricate link between the nanometer correlation length scale, the energy scale for octahedral tilt fluctuations, and the coefficient of thermal expansion in ScF_3 . We then investigate the breakdown of the rigid limit and propose a resolution to an outstanding debate concerning the role of molecular rigidity in strong NTE materials.

DOI: [10.1103/PhysRevB.94.214102](https://doi.org/10.1103/PhysRevB.94.214102)

Structural negative thermal expansion (NTE) is a fascinating and growing field of condensed matter physics due to the rarity of the phenomenon, a stunning display of unconventional lattice dynamics, and the strong potential for structural applications where dimensional stability is required. This type of NTE phenomenon refers to the unusual tendency for materials to shrink when heated as a property of bond network topology and the associated fluctuations [1–3], which is distinct from NTE arising from electronic or magnetic instabilities observed in Invar [4] and valence transitions [5]. Recently, the nonmagnetic ionic insulator ScF_3 has drawn particularly intense attention in the chemistry community [6] as the first instance of a perovskite-structured material with strong, isotropic, and thermally persistent NTE, a distinction which no longer appears to be an isolated case [7]. ScF_3 displays strong NTE ($-15 \text{ ppm/K} < \alpha_L < 0$) over a temperature window of 1000 K, but is also unusual in its lack of any type of phase transition whatsoever within the solid state: The system retains a small, four-atom (formula) unit cell at all temperatures below the solid-liquid phase boundary $T < 1800 \text{ K}$.

Work aimed to develop a mechanistic understanding of the NTE effect in ScF_3 and similar behavior in the more complex open-framework NTE compound ZrW_2O_8 has compared complementary experiments to simulations with an outstanding debate as to the role of molecular rigidity in the NTE mechanism. One may naturally expect such an approach to apply when considering the hierarchy of energy scales within the lattice degrees of freedom. For transition metal perovskites, these break down as bond-stretching motion at high (50–100 meV) energy, bond-bending motion at medium (20–50 meV) energy, and a lower (1–3 meV) set of external modes described as the coordinated motion of units which respect the internal dimensions of molecular subunits such as the ScF_6 octahedra [8–10]. This tiered energy structure suggests that some normal modes are frozen out at temperatures where the boson population is much lower than one. For example, the lowest zone-center optical mode in ScF_3 observed [11]

at 24 meV has a boson population $n \simeq 0.62$ at 300 K, suggesting that these uniform intramolecular distortions are frozen out even at room temperature while the much softer (3.6 meV [12]) intermolecular degrees of freedom on the zone boundary dominate with a population $n \simeq 2$. These estimates suggest that some progress on the problem may be developed by using a view of lattice dynamics which shifts focus from the atom to molecular subunits as the basic building blocks may be appropriate to describe certain phenomena such as NTE. Building on this idea, some researchers find an adequate description of NTE in terms of rigid molecular units which draw in the lattice when thermally activated, with still finer points of debate on which senses of motion are appropriate for which particular system [13–15], or across which momentum manifolds rigid external modes exist [16]. Others have suggested that molecular rigidity is neither necessary nor favorable as an NTE mechanism [15,17–19].

Separately from any consideration of NTE, studies of the perovskite space group landscape show that the cubic open perovskites in the $Pm\bar{3}m$ structure such as ScF_3 and ReO_3 can undergo coordinated tilt patterns [20] of rigid octahedra. The associated soft modes reside on one-dimensional manifolds along the simple cubic Brillouin zone (BZ) edges. Recent inelastic x-ray scattering (IXS) work analyzing the temporal correlations of single-crystal ScF_3 has indeed shown the presence of a soft mode manifold circumscribing the BZ edges [12]. Here we extend this study using high-energy resolution diffuse x-ray scattering and find that these soft modes imply two-dimensional (2D) spatial correlations associated with NTE. In our analysis, we exploit the structural simplicity of ScF_3 and agnostically assess the viewpoint of molecular rigidity. In what follows, we develop a mathematical model with rigid constraints and compare to recent and existing data. We show explicitly that a strictly rigid network is both unphysical and inconsistent with observations, but a picture of locally rigid correlations is capable of unifying disparate experimental observations within a simple and intuitive approach.

Figure 1(b) shows a momentum surface of the elastic x-ray intensity in single-crystal ScF_3 taken at $T = 300 \text{ K}$ with a high-

*jason.hancock@uconn.edu

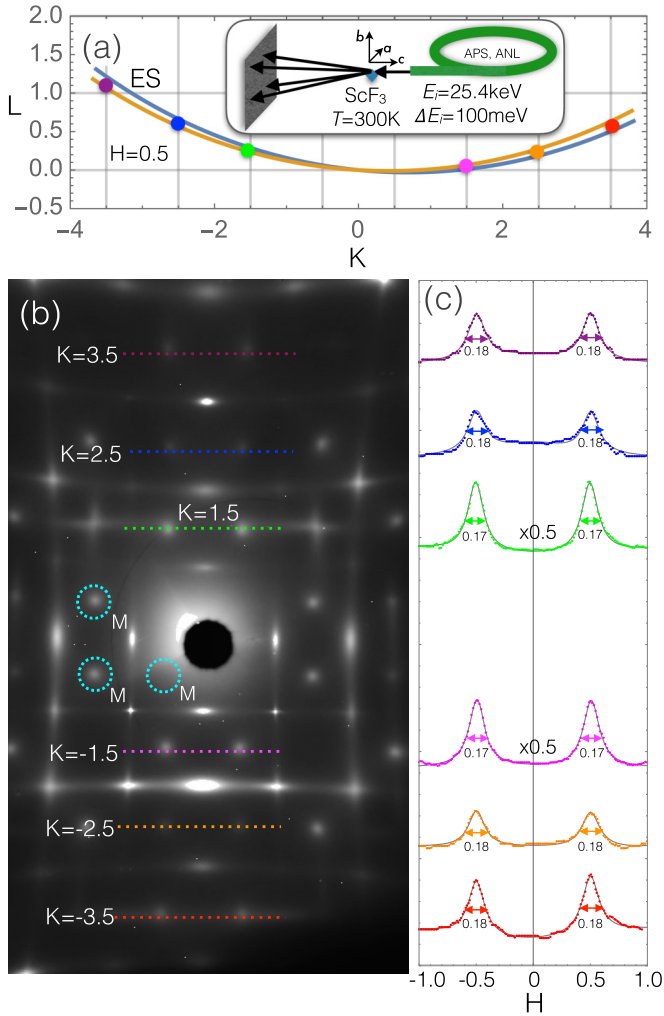


FIG. 1. (a) Inset: Experimental geometry for the diffuse scattering experiments in single-crystal ScF_3 . The main panel shows a $H = 0.5$ cross section of the Ewald sphere. Blue and orange arcs indicate the extrema of the crystal rocking angle. (b) Diffuse scattering intensity collected using the experimental geometry in (a). Midzone intensity at M points are indicated by dashed circles and are found in almost every BZ. Dashed lines indicate cuts through the intensity patterns shown in (c). Each cut in (c) is taken at an equivalent K value but corresponds to a different L value. The negligible change in widths is strong evidence of 2D spatial correlations.

resolution incident beam and an image plate at sector 30-ID-C of the Advanced Photon Source (APS), Argonne National Laboratory (ANL). Momentum space is indexed to the simple cubic four-atom unit cell using Miller indices HKL and the surface sampled is an Ewald sphere (ES) shown approximately in Fig. 1(a). The ES samples approximately the $HK0$ plane near the origin, but finite curvature extends the sampled volume along the L direction. Cuts in the H (horizontal) direction are taken at equivalent half-integer values of K , but correspond to different L positions along the scattering rods, as described in Fig. 1(a). Lorentzian fits to these transverse cuts produce widths corresponding to about $1/0.18$ – 5.5 unit cells, independently of where the cut is made along the M - R branch. We conclude that scattering rods are present along the BZ edges, reflecting short-range 2D nanoscale correlations of

order 6 unit cells. The weak dispersion of optic modes reported previously [12] along this cut further suggests a decoupling of planar correlations corresponding to 2D coordinated rotations. In terms of microscopic interactions, the lack of dispersion along the M - R branch can be interpreted as a small steric barrier—the energy cost to twist the Sc-F-Sc bond is very low. This produces an effective decoupling of the phase of coordinated octahedral motion in one plane with another.

Figure 2(b) shows the simple cubic BZ of ScF_3 with breakouts indicating the nature of the correlated motion comprising M - R zone boundary modes. The experimentally observed decoupling of coordinated rotations within planar manifolds suggests there is prominent importance of the lattice dynamics of a 2D section, shown in Figs. 2(c) and 2(d). A model consisting of stiff diamonds connected by hinged joints shown in Figs. 2(c) and 2(d) appears in numerous contexts in the literature describing the NTE phenomenon as a physical model wherein one may see that the collective motion of a rigid network could generically provide a NTE influence [21–23]. The diamonds could represent metal-anion octahedra in the structural NTE perovskites ScF_3 or ReO_3 , but the idea has been used to schematically describe more complex structures [21–25]. In what follows, we momentarily enforce the rigidity of the molecular units in an analysis of this two-dimensional constrained lattice model (2D CLM) to study the rigid limit expectations before comparing to experiment in order to provide insights into the limitations and strengths of rigid models in the NTE problem.

The 2D CLM consists of corner-linked diamonds with coordinate origin at its center of mass (COM). The $N_\diamond = N_x N_y$ diamonds are attached by hinged joints, so that their motional degrees of freedom are constrained. The CLM is isostatic, or marginally constrained, in the sense that even in the thermodynamic limit, there is exactly one internal degree of freedom: a staggered rotation of each diamond by an angle θ . Increasing θ from zero contracts the lattice from initial area A_0 to an area $A_0 \cos^2 \theta$, and thermal activation of this collective mode is often attributed as the origin of NTE [21–25]. Efforts to expand this model to field theories which respect the high-energy constraints of bond-stretch and bond-bend degrees of freedom include mimicking polyhedral pliancy through a split-atom approach [8], by lowering the degree of constraint [3,9], or permitting some diamonds to be replaced by springs [10], and unusual properties such as NTE are found in each case.

When there is no staggered rotation, $\theta = 0$, and a diamond center can be located at position $\vec{r}(\theta = 0) = (n_x, n_y)a_0$. When $\theta \neq 0$, the distance between neighboring diamond centers is reduced by a multiplicative factor $\cos \theta$ and each position vector is scaled similarly $\vec{r}(\theta) = (n_x, n_y)a_0 \cos \theta$ with velocity vector $\dot{\vec{r}}(\theta) = -(n_x, n_y)a_0 \dot{\theta} \sin \theta$. The velocity vectors of each diamond always point directly toward or away from the COM. The total translational kinetic energy summed over all diamonds in the crystal is

$$K_\diamond^{\text{trans}} = \frac{1}{2} I_c \dot{\theta}^2 \sin^2 \theta,$$

where $I_c = \sum_{n_x, n_y} m_\diamond [(n_x a_0)^2 + (n_y a_0)^2]$ is the moment of inertia of a similar crystal where diamonds are replaced by points, each of mass m_\diamond .

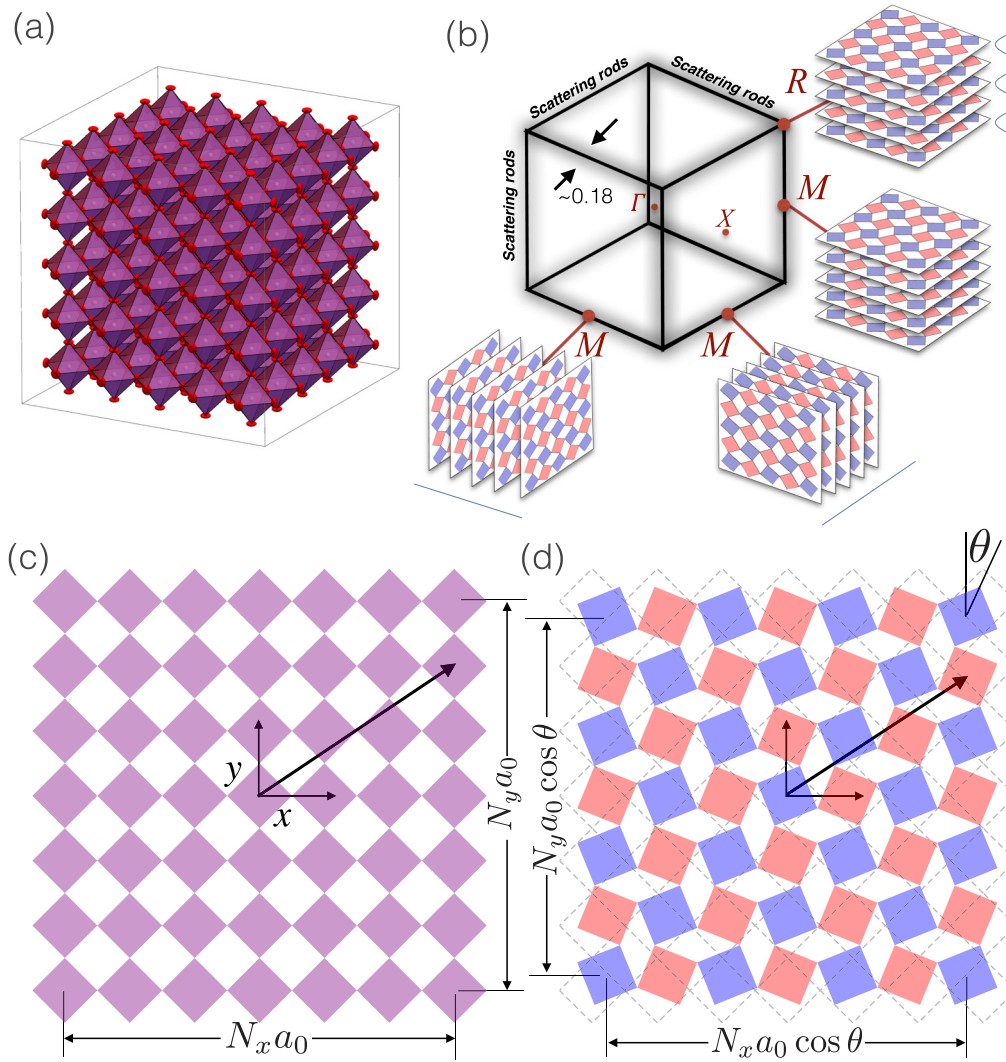


FIG. 2. (a) A $5 \times 5 \times 5$ crystallite of ScF_3 in the average structure (125 octahedra). (b) The hollow cube shows the simple cubic BZ with shaded regions indicating the positions of observed scattering rods from the data in Fig. 1. Breakouts show possible real-space staggered rotation patterns which preserve internal octahedral dimensions at the indicated high-symmetry momentum-space points. Red and blue shading in the diamonds indicate equal but opposite magnitudes of rotation. (c) A 2D CLM which supports a single floppy mode (FM). As a result of the constraints, a staggered rotation by an angle θ in (d) causes a shortening of the vector locating each diamond by a factor $\cos \theta$.

Including the rotational kinetic energy of each diamond and summing, the total kinetic energy of the 2D CLM is

$$K = \frac{1}{2} N_{\diamond} I_{\diamond} \dot{\theta}^2 + \frac{1}{2} I_c \dot{\theta}^2 \sin^2 \theta = \frac{1}{2} N_{\diamond} I_{\diamond} \dot{\theta}^2 (1 + k^2 \sin^2 \theta),$$

where $k = \sqrt{\frac{I_c}{N_{\diamond} I_{\diamond}}} = \sqrt{\gamma N_{\diamond}}$ and γ depends on the aspect ratio of the crystal and mass distribution for the diamonds ($\simeq 1.79$ for a square crystallite of ScF_3). Finally, we introduce the lowest Fourier component of an intermolecular bond-bending potential at the hinges $\kappa(1 - \cos \theta)$ to stiffen the structure from collapse. Microscopically, this influence arises from a competition between mutual repulsion of like charges including dipolar contributions and anion polarizability and is considered low for trifluorides with a large B -site atomic radius such as Sc [26]. The total energy, expanded for a small angle to the harmonic case, is then

$$E = \frac{1}{2} N_{\diamond} I_{\diamond} (1 + k^2 \theta^2) \dot{\theta}^2 + \frac{1}{2} N_b \kappa \theta^2, \quad (1)$$

where $N_b \simeq 2N_{\diamond}$ is the total number of intermolecular linkages. One may view Eq. (1) as a generalization of a harmonic oscillator ($k \rightarrow 0$) describing a residual degree of freedom resultant from integrating out high-energy bond-stretch and bond-bend degrees of freedom.

Significantly, the total effective inertia of the FM has a rotational part (the first term) which scales with system size in an *intensive* way ($\propto N_{\diamond}$), while the translational kinetic energy scales *extensively* ($I_c \propto N_{\diamond}^2$). As the thermodynamic limit is approached, molecular units at the boundary of a free crystallite must traverse macroscopic distances within a single FM cycle while experiencing enormous force gradients, pointing to a necessary breakdown of rigidity and falsifies the rigid approach on physical grounds. A homogeneous FM in an infinite system therefore has an infinite kinetic energy density, and the effect favors inhomogeneous spatial textures through intramolecular deformations at a penalty of elastic potential energy. In what follows we entertain the possibility

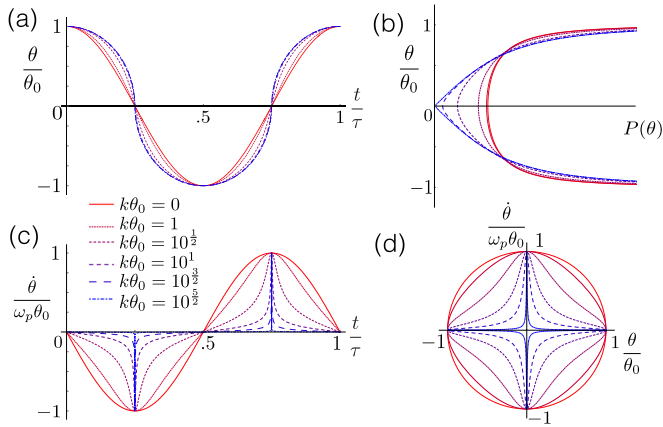


FIG. 3. (a)–(d) show classical solutions for $\theta(t)$ which follow from Eq. (3). These are plotted for different values of $k\theta_0$, which uniquely quantifies the anharmonic behavior. The time axes in (a) and (c) are scaled by the FM period.

that the nanoscale correlations we observe are a signature of such a breakdown, as an alternative approach to a conventional phonon population of optical modes.

In the limit of small-angle and large system size (k), one can integrate (1) to find

$$\frac{(t - t_0)^2}{(k\theta_0/\omega_p)^2} + \frac{\theta^2}{\theta_0^2} = 1,$$

where θ_0 is the amplitude and $\omega_p = \sqrt{N_b\kappa/N_\circ I_\circ}$ is the angular frequency of small oscillations in the limit $k = 0$. Several aspects of the thermodynamic FM are distinct from the harmonic case: (i) The period $\tau = \frac{4k\theta_0}{\omega_p} = 4\theta_0\sqrt{\frac{I_c}{N_b\kappa}}$ diverges and is proportional to the amplitude of oscillation, (ii) the time-averaged classical probability distribution $P(\theta)$ dwells much longer near the extrema than the harmonic case, and (iii) the system spends a vanishingly small time in the average structure $\theta = 0$ [Fig. 3(b)]. The latter two points are apparent in recent molecular dynamics simulations of ScF_3 that reach similar surprising conclusions of nearly vanishing probability for straight Sc-F-Sc bonds at elevated temperatures [27]. A physical expression of this peculiar distribution in the present model can be seen in the time-averaged area, related to the moments of this distribution, $\langle A \rangle_t = A_0 \langle \cos^2 \theta(t) \rangle_t = A_0(1 - \eta\theta_0^2)$, where $\eta = 1/2$ for the sinusoidal $k = 0$ case and $\eta = 2/3$ for the thermodynamic limit $k \rightarrow \infty$ (see the Supplemental Material [28]), showing that the strain dynamics of the 2D CLM enhances NTE over its harmonic counterparts. The lessons from these results on the CLM is that the collective motion of the dilating FM is slow and anharmonic, dwelling near extrema as a feature of its dynamics.

We note that the dispersion away from the zone boundaries is very steep, approaching the longitudinal acoustic velocity, suggesting the dominant importance of the BZ edge modes to NTE. We are therefore positioned to compare the experimental $a(T)$ for ScF_3 with that of an uncorrelated stack of $N_s = N_x^2$ thermally averaged 2D CLMs of area $A(T) = A_0 \langle \cos^2 \theta \rangle_T \simeq A_0(1 - \langle \theta^2 \rangle_T)$. The lattice parameter of the stack is then $a(T) = a_0 \langle \cos^2 \theta \rangle_T^{1/3} \simeq a_0(1 - \langle \theta^2 \rangle_T/3)$, where we sum over

the BZ edges to obtain

$$\langle \theta^2 \rangle_T = \frac{1}{Z} \int \theta^2 e^{-\beta H} dk_z d\theta dL_\theta = \frac{2k_B T}{N_b \kappa} \frac{1}{1 + \frac{K_0(\delta)}{K_1(\delta)}}, \quad (2)$$

$\beta = 1/k_B T$, Z is the classical partition function, $\delta = \frac{N_b \kappa}{4k^2 k_B T} = \frac{I_c \omega_p^2}{4k_B T \gamma}$, and $K_n(\delta)$ is the order n modified Bessel function of the second kind.

Using the inertial parameters for ScF_3 and $a_0 = 4.0285 \text{ \AA}$, Figs. 4(a) and 4(b) show plots of $a(T)$ and the transverse anion thermal parameter $U_{33}(T) = (a_0/2)^2 \langle \theta^2 \rangle_T$ determined from the model along with existing experimental data [12, 18] using the observed $N_x = 5.5$ for different values of ω_p .¹ Best agreement is met when $\hbar\omega_p \simeq 1.6 \text{ meV}$, which is similar in magnitude to the observed branch energy at low temperature (1.2–1.4 meV) and somewhat lower than the observed values at ambient temperature (3.4–3.6 meV). We remark that existing computational work gives mode energies ranging from 3 to 6.5 meV [11, 17, 18], and that inclusion of other low-energy modes off of the high-symmetry cut is expected to raise this effective energy scale somewhat.

Remarkably, this analysis has the implication of an intricate link between the following experimental quantities: (i) the length scale ~ 6 unit cells we observe in diffuse x-ray scattering, (ii) the energy scale $\sim 1 \text{ meV}$ for the M - R branch reported using IXS, and (iii) the degree of dimensional fluctuation measured through the coefficient of thermal expansion measured using x-ray diffraction. Recent purely theoretical analyses of square and kagome lattices crossing the isostatic limit using different approaches have also pointed to emergent nanometer length scales [29–31]. In contrast, the present results use a simple approach motivated by experimental observations to relate disparate experimental observables in a real material system.

Recent classical molecular dynamics simulations and general arguments have suggested the strict rigidity of molecular units is not possible or necessary for NTE [15, 17–19], fully consistent with the finite correlation length implied by our experiments and divergent kinetic energy density in the thermodynamic limit of the CLM. Here we propose a mechanism of strain relief and kinetic energy lowering consistent with experiments, the quantized nature of the vibrational spectrum, and the hierarchy of stiffness present in the bond patterns. The pileup of translational kinetic energy at the boundary of a dilating region implied by molecular rigidity could be alleviated by introducing bond-bend intramolecular polyhedral deformations. Within a FM cycle, the separation between the edges of two adjacent, dilating nanoregions is minimized if the phases of oscillation φ_1 and φ_2 differ by $\varphi_1 - \varphi_2 = \pm\pi/2$. These two choices keep the edges in contact without parting the junction and lower the translational kinetic energy significantly. We can demonstrate this savings by considering the kinetic energy of a homogeneous excitation of a 2D CLM in a long, narrow solid shown in Fig. 4,

¹We note the offset in $U_{33}(T)$ can be a result of residual strain or disorder in the experimental data and remark that the slope is of similar size to the model when $\hbar\omega_p = 1.6 \text{ meV}$.

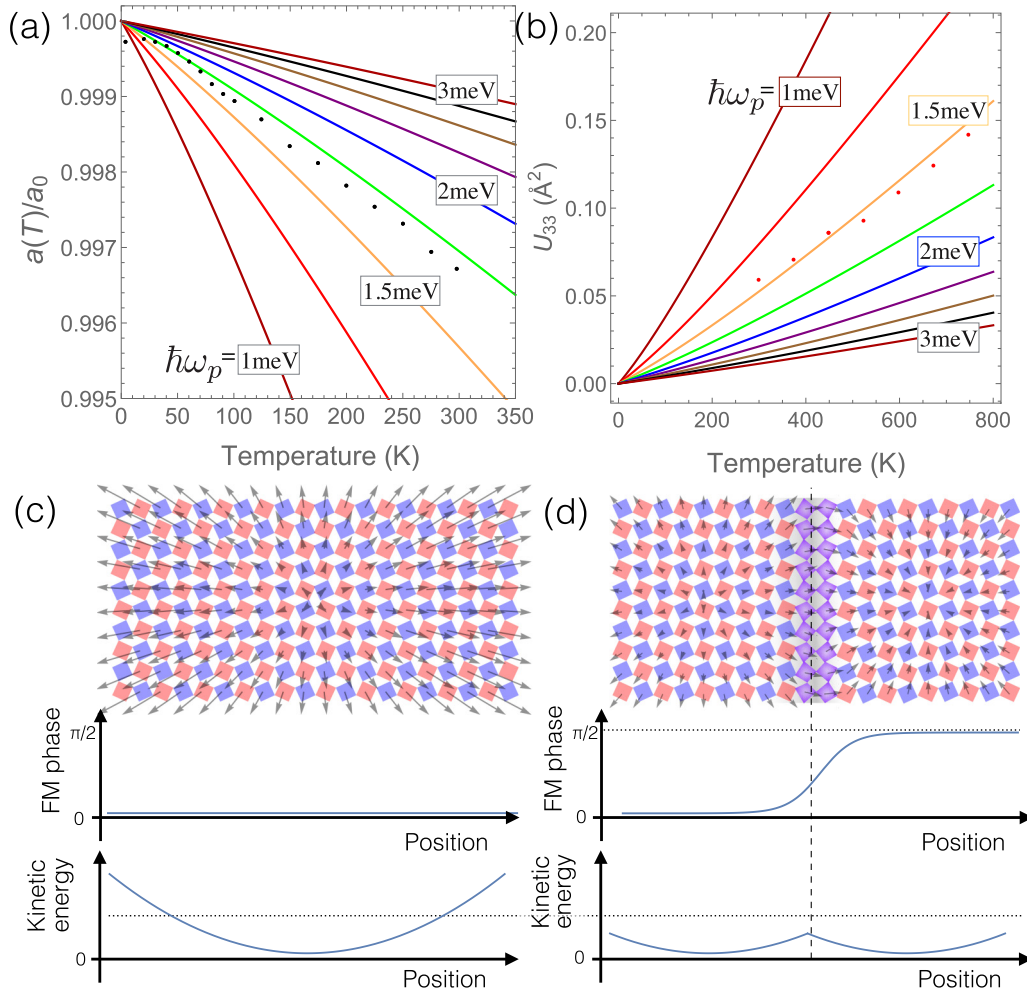


FIG. 4. (a) Lattice parameter of ScF_3 below $T = 300$ K from Ref. [12]. (b) Transverse fluorine thermal parameter determined from x-ray pair density function analysis [18]. Superimposed on (a) and (b) are the corresponding quantities from (2) using $N_x = 5.5$ for varying values of $\hbar\omega_p$. (c) Velocity field superimposed on a homogeneously excited FM, with phase and kinetic energy below. (d) shows the significant kinetic energy lowering when a $\pi/2$ defect is introduced.

$N_x \times N_y$, with $N_x \gg N_y$ is given in (1) with moment of inertia $I_c^{(1)} = 2m_\circ a^2 N_x^3 N_y / 3$. An inhomogeneous excitation with a locally straight domain wall at the origin separating a region of FM phase 0 (maximum volume) for $x < 0$ and FM phase $\pi/2$ (minimum volume) for $x > 0$ has an effective crystal moment of inertia which is four times lower $I_c^{(2)} = m_\circ a^2 N_x^3 N_y / 6 = \frac{1}{4} I_c^{(1)}$. A similar calculation for two semiplanes in contact gives $I_c^{(2)} = \frac{1}{2} I_c^{(1)}$, in any case lowering the energy. The interface between these regions must feature excited optical modes with an elastic energy penalty made possible by the enormous lowering of translational kinetic energy.

The molecular velocity field in this scenario may be described as monopole-antimonopole pairs. The topological defects proposed here are resultant from the alleviation of strain at the interface and are protected at a $\simeq 20$ meV scale. While details of a possible superstructure await further experiments and modeling, we identify a large kinetic energy lowering occurs through the formation of a $\pi/2$ phase slip defect, which may pose intrinsic challenges to theories which embark with a classical approach. For a large single 2D planar section, the $\pm\pi/2$ phase slip could occur in multiple

ways, potentially benefitting the stability of the proposed excitations. A three-dimensional extension of such defect field is beyond the scope of the present work, but may give rise to nontrivial topological textures in the phase field of the FM, raising the interest in lattice systems with unconventional dynamics. Future time-resolved and coherent x-ray scattering experiments are likely to address the phase relationship intrinsic to the nanoscale correlations in NTE materials.

The authors would like to acknowledge valuable conversations with Richard Brierley, Joshua Deutsch, Gian Guzman-Verri, and Peter Littlewood. Support for this project was provided by National Science Foundation Award No. DMR-1506825. Work at Argonne National Laboratory is supported by the U.S. Department of Energy, Office of Basic Energy Sciences under Contract No. DE-AC02-06CH11357. The construction of HERIX was partially supported by the NSF under Grant No. DMR-0115852. C.A.O. acknowledges support from the Treibic family scholarship, managed by the Office of Undergraduate Research at the University of Connecticut.

- [1] A. P. Giddy, M. T. Dove, G. S. Pawley, and V. Heine, *Acta Crystallogr., Sect. A* **49**, 697 (1993).
- [2] A. Ramirez, C. Broholm, R. Cava, and G. Kowach, *Physica B (Amsterdam)* **280**, 290 (2000).
- [3] Z. Schlesinger, J. A. Rosen, J. N. Hancock, and A. P. Ramirez, *Phys. Rev. Lett.* **101**, 015501 (2008).
- [4] C. E. Guillaume, in *Nobel Lectures, Physics 1901–1921* (Elsevier, Amsterdam, 1967), pp. 1–16.
- [5] M. Azuma, W.-t. Chen, H. Seki, M. Czapski, S. Olga, K. Oka, M. Mizumaki, T. Watanuki, N. Ishimatsu, N. Kawamura *et al.*, *Nat. Commun.* **2**, 347 (2011).
- [6] B. K. Greve, K. L. Martin, P. L. Lee, P. J. Chupas, K. W. Chapman, and A. P. Wilkinson, *J. Am. Chem. Soc.* **132**, 15496 (2010).
- [7] J. C. Hancock, K. W. Chapman, G. J. Halder, C. R. Morelock, B. S. Kaplan, L. C. Gallington, A. Bongiorno, C. Han, S. Zhou, and A. P. Wilkinson, *Chem. Mater.* **27**, 3912 (2015).
- [8] P. Sollich, V. Heine, and M. T. Dove, *J. Phys.: Condens. Matter* **6**, 3171 (1994).
- [9] M. E. Simon and C. M. Varma, *Phys. Rev. Lett.* **86**, 1781 (2001).
- [10] Y. He, V. Cvetkovic, and C. M. Varma, *Phys. Rev. B* **82**, 014111 (2010).
- [11] S. Piskunov, P. A. Žguncs, D. Bocharov, A. Kuzmin, J. Purans, A. Kalinko, R. A. Evarestov, S. E. Ali, and F. Rocca, *Phys. Rev. B* **93**, 214101 (2016).
- [12] S. U. Handunkanda, E. B. Curry, V. Voronov, A. H. Said, G. G. Guzman-Verri, R. T. Brierley, P. B. Littlewood, and J. N. Hancock, *Phys. Rev. B* **92**, 134101 (2015).
- [13] D. Cao, F. Bridges, G. R. Kowach, and A. P. Ramirez, *Phys. Rev. Lett.* **89**, 215902 (2002).
- [14] M. G. Tucker, A. L. Goodwin, M. T. Dove, D. A. Keen, S. A. Wells, and J. S. O. Evans, *Phys. Rev. Lett.* **95**, 255501 (2005).
- [15] A. Sanson, *Chem. Mater.* **26**, 3716 (2014).
- [16] A. K. A. Pryde, M. T. Dove, and V. Heine, *J. Phys.: Condens. Matter* **10**, 8417 (1998).
- [17] C. W. Li, X. Tang, J. A. Muñoz, J. B. Keith, S. J. Tracy, D. L. Abernathy, and B. Fultz, *Phys. Rev. Lett.* **107**, 195504 (2011).
- [18] L. Hu, J. Chen, A. Sanson, H. Wu, C. Guglieri Rodriguez, L. Olivi, Y. Ren, L. Fan, J. Deng, and X. Xing, *J. Am. Chem. Soc.* **138**, 8320 (2016).
- [19] J. T. Schick and A. M. Rappe, *Phys. Rev. B* **93**, 214304 (2016).
- [20] P. M. Woodward, *Acta Crystallogr., Sect. B* **53**, 32 (1997).
- [21] C. Lind, *Materials* **5**, 1125 (2012).
- [22] J. N. Grima, P. S. Farrugia, R. Gatt, and V. Zammit, *Proc. R. Soc. London, Ser. A* **463**, 1585 (2007).
- [23] K. Takenaka, *Sci. Technol. Adv. Mater.* **13**, 013001 (2012).
- [24] J. Tao and A. Sleight, *J. Solid State Chem.* **173**, 442 (2003).
- [25] W. Miller, C. W. Smith, D. S. Mackenzie, and K. E. Evans, *J. Mater. Sci.* **44**, 5441 (2009).
- [26] P. B. Allen, Y.-R. Chen, S. Chaudhuri, and C. P. Grey, *Phys. Rev. B* **73**, 172102 (2006).
- [27] P. Lazar, T. Bučko, and J. Hafner, *Phys. Rev. B* **92**, 224302 (2015).
- [28] See Supplemental Material at <http://link.aps.org/supplemental/10.1103/PhysRevB.94.214102> for derivations relevant to the work.
- [29] A. Souslov, A. J. Liu, and T. C. Lubensky, *Phys. Rev. Lett.* **103**, 205503 (2009).
- [30] X. Mao, N. Xu, and T. C. Lubensky, *Phys. Rev. Lett.* **104**, 085504 (2010).
- [31] K. Sun, A. Souslov, X. Mao, and T. C. Lubensky, *Proc. Natl. Acad. Sci. USA* **109**, 12369 (2012).